Sensors and Materials, Vol. 36, No. 12 (2024) 5309–5321
MYU Tokyo

S & M 3869

Sensor Fault Detection Using Spatial-temporal Correlation Fusion Algorithm

Yuan Wang,[1] Nuobin Zhang,[2,3*] Huijie Wang,[1] Chunfang Pan,[1] and Jiarui Li[2,3]

[1]Chuxiong Power Supply Bureau, Yunnan Power Grid Co., Ltd., Chuxiong 675000, P.R. China
[2]Yunnan Power Grid Energy Investment Co., Ltd., Kunming 650000, P.R. China
[3]Faculty of Civil Aviation and Aeronautical, Kunming University of Science & Technology, Kunming 650500, P.R. China

(Received May 3, 2024; accepted December 13, 2024)

Keywords: wireless sensor network, spatial-temporal correlation, fusion algorithm, adaptive weights

With the profound changes in transportation and energy, the integration of new energy electric vehicles into the power grid will generate a large amount of data. Sensors are deployed in the coupling environment of a transportation network and a power grid to transmit accurate monitoring data. Aiming at sensors that generate faults under the coupling interaction between a distribution network and a transportation network, in this paper, we propose a fault sensor node judgment method based on the spatial-temporal correlation fusion algorithm (FA). First, the cubic exponential smoothing (CES) algorithm of the time attribute and the piecewise least squares (PLSE) algorithm of the spatial properties are used to predict the temperature, humidity and voltage data monitored by the sensors. Then, according to the error size, the adaptive weight adjustment method is used to find the optimal weight value, and the FA model is obtained, so as to gain more accurate detection results. Finally, by comparing the predicted value with the set confidence interval, the identification of the fault sensor node is demonstrated. The results showed that the detection model proposed in this study has excellent fault sensor node detection performance. For the prediction results of the temperature data of the sensor, the fit accuracies of FA are 45.1 and 77.4% higher than those of ES and PLSE, respectively, which has certain practical significance.

1. Introduction

The increasing adoption of electric vehicles has deepened the integration between transportation networks and the power grid, fostering mutual influence between energy dynamics and transportation systems. Deploying sensors in relevant environments enables the real-time monitoring of traffic flow, power consumption, and equipment operation.(1) Wireless sensor networks, renowned for their scalability, self-organization, and reliability, have found diverse applications, including military operations,(2) environmental surveillance,(3) and healthcare.(4) However, the sensors manufactured today generally have the characteristics of low cost and intelligence, and are usually deployed in harsh environments, and the probability of

*Corresponding author: e-mail: 2972322553@qq.com
https://doi.org/10.18494/SAM5336

ISSN 0914-4935

sensor failure is considerably raised by the effects of environment conditions. In the scenario of extensive and complex traffic network and power grid coupling, the deployed sensor monitors a large number of parameters, and the data transmission and storage are prone to errors, resulting in the misjudgment of the fault node. It is very important to monitor the state of the electric vehicle by deploying the sensor to achieve a reasonable scheduling of power resources and balance of the power demand. Therefore, the fault detection method of sensor network nodes has become a hot research topic in this field.[5] Fusion algorithms can be suitable for applications in various fields by combining the advantages of different algorithms to enhance the robustness, reliability and adaptability of the system.[6] In this study, we employed a spatial-temporal correlation fusion algorithm (FA) to integrate sensor data from diverse dimensions, thereby augmenting the precision of numerical predictions for sensor nodes.[7,8]

Fault detection in wireless sensor networks involves monitoring and identifying the abnormal or faulty states of sensor nodes, a critical process for ensuring network reliability and effectiveness. Current research primarily focuses on the soft faults of sensor nodes, emphasizing fault node detection. Methods of sensor node fault detection include the use of distributed and centralized fault diagnosis algorithms, packet loss analysis, transmission time comparison, and others.[9–12] While these methods enhance detection accuracy compared with traditional approaches, they often demand high system hardware complexity and stability, leading to the significant consumption of computing and network resources.

In this study, we focus on detecting sensor fault nodes by identifying abnormal data. Initially, analysis reveals nonlinear time series characteristics of collected sensor data. The cubic exponential smoothing (CES) algorithm model can quickly capture the trend and seasonal changes in the data, especially for the analysis of time series data with clear trends and seasonal laws, and improve the accuracy of prediction.[13,14] Additionally, the piecewise least squares (PLSE) method is employed to fit sensor data. However, in dealing with nonlinear relationships, the single least squares method struggles to approximate the data accurately. Segmentation improves model robustness by adapting to changing data trends and enhancing resilience to outliers.[15,16]

Finally, to solve the problem that the fault sensor nodes are difficult to detect in the actual scene of the electric vehicle incorporated into the power grid, in this study, we combined the above two sensor fault node detection methods based on the time and space attribute characteristics of the data collected by the sensor nodes. A FA model based on spatial-temporal correlation is introduced. Through the two-way detection using the CES algorithm with the time attribute and the PLSE method with the spatial properties, a better detection and recovery effect is achieved.

2. Spatial-temporal FAs

2.1 CES algorithm of time characteristic

The CES model assigns weights to historical data on the basis of their proximity to the current moment, giving higher weight to data closer to the present and lower weight to data

further away. This weighting scheme ensures the rationality of prediction results. The formula is expressed as

$$F_t^{(3)} = \alpha F_t^{(2)} + (1-\alpha)F_{t-1}^{(3)}. \tag{1}$$

Here, $F_t^{(3)}$ is the smooth value obtained at time t, $F_{t-1}^{(3)}$ is the smooth value obtained at time $t-1$, its superscript (3) expresses a CES, α is the smoothing coefficient, and the value range is $\alpha \in (0,1)$.

It is concluded that the model of predicting $E_{\hat{Q}_{t+T}}$ of the observation data of sensor Q at a future time by the CES algorithm is

$$E_{\hat{Q}_{t+T}} = A_t + B_t T + C_t T^2. \tag{2}$$

The calculation formula for each coefficient in the prediction model is

$$\begin{cases} A_t = 3F_t^{(1)} - 3F_t^{(2)} + F_t^{(3)}, \\ B_t = \dfrac{\alpha}{2(1-\alpha)^2}\left[(6-5\alpha)F_t^{(1)} - 2(5-4\alpha)F_t^{(2)} + (4-3\alpha)F_t^{(3)}\right], \\ C_t = \dfrac{\alpha^2}{2(1-\alpha)^2}\left[F_t^{(1)} - 2F_t^{(2)} + F_t^{(3)}\right]. \end{cases} \tag{3}$$

In the above formula, T represents the period of the sequence.

2.2 PLSE method of spatial properties

2.2.1 Least squares estimation (LSE)

It is assumed that the following two sensor data sequences $Q = (Q_1, Q_2, ..., Q_N)$ and $Z = (Z_1, Z_2, ..., Z_N)$ with spatial correlation are obtained. They are the temperature data sequence of sensor Q and the humidity data sequence of sensor Z, respectively. The calculation formula is

$$L_{\hat{Q}(z)} = \bar{m}_Q + \frac{\lambda_{Qz}}{\lambda_z}(Z - \bar{m}_z), \tag{4}$$

where $L_{\hat{Q}(Z)}$ is the predicted value of the temperature of sensor Q based on the humidity data set of sensor Z, $\bar{m}_Q$ is the mean value of the temperature data of sensor Q, $\bar{m}_Z$ is the mean value of the humidity data of sensor Z, λ_Z is the variance of the humidity data value of sensor Z, and λ_{QZ} is the covariance of the data between the temperature of sensor Q and the humidity of sensor Z. The calculation formula is

$$\begin{cases} \bar{m}_Q = \dfrac{1}{N}(Q_1 + Q_2 + ... + Q_N), \\ \bar{m}_Z = \dfrac{1}{N}(Z_1 + Z_2 + ... + Z_N), \\ \lambda_Z = \mathrm{var}(Z) = \dfrac{1}{N-1}\sum\limits_{i=1}^{N}(Z_i - \bar{m}_Z)^2, \\ \lambda_{QZ} = \mathrm{cov}(Q,Z) = \dfrac{1}{N-1}\sum\limits_{i=1}^{N}(Q_i - \bar{m}_Q). \end{cases} \tag{5}$$

2.2.2 PLSE

First, the regression equation function is selected as $y = a + bx$, where a is the intercept and b is the slope. For N sets of data (X_i, Y_i) (i = 1, 2, ..., N) in the dataset, we define the error term as

$$Q = \sum_{i=1}^{N}(Y_i - Y)^2 = \sum_{i=1}^{N}(Y_i - a - bX_i)^2. \tag{6}$$

Then, the data sequence is divided into k groups:

$$\begin{aligned} N_1 &= (X_{11}, Y_{11}), (X_{12}, Y_{12}), \ldots, (X_{1m_1}, Y_{1m_1}), \\ N_2 &= (X_{21}, Y_{21}), (X_{22}, Y_{22}), \ldots, (X_{2m_2}, Y_{2m_2}), \\ &\ldots \\ N_k &= (X_{k1}, Y_{k1}), (X_{k2}, Y_{k2}), \ldots, (X_{km_k}, Y_{km_k}). \end{aligned} \tag{7}$$

The fit error is related to the k groups and the value of the segmentation point $(m_1, m_2, ..., m_{k-1})$, and then the piecewise fit of the data sequence is realized in accordance with the principle of minimum overall fit error.

The overall fit error is

$$Q^k = \sum_{i=1}^{m_1}(Y_i - a_1 - b_1 X_i)^2 + ... + \sum_{i=m_{k-1}+1}^{N}(Y_i - a_k - b_k X_i)^2. \tag{8}$$

We choose the best segmentation point as $(m_1, m_2, ..., m_{k-1})$ when Q^k takes the minimum value of $Q^k{}_{min}$.

2.3 FA

By combining Eqs. (2) and (4), the equation of the FA can be obtained as

$$\widehat{Q}_t = \mu \cdot E_{\widehat{Q}_t} + \nu \cdot L_{\widehat{Q}_t}, \tag{9}$$

where the predicted value of the improved FA for sensor Q at time t is $\hat{Q}_t$, μ represents the weight coefficient given by the time attribute detection algorithm in the prediction, v represents the weight coefficient given by the spatial properties detection algorithm in the prediction, and $\mu \in (0,1]$, $\nu \in (0,1]$. In the calculation, the predicted value of the Q sensor calculated using the CES algorithm at time t is $E_{\hat{Q}_t}$ and $L_{\hat{Q}_t}$ is the predicted value of the sensor data sequence calculated by the PLSE method at time t.

The overall flow chart of the FA is shown in Fig. 1.

3. Parameter Selection

It can be seen from the calculation formula [Eq. (9)] of the FA that the selection of the smoothing coefficient, segmentation interval, and weight coefficient determines the accuracy of the judgment of abnormal data.

3.1 Smoothing coefficient in CES algorithm

The smoothing coefficient (α) directly affects the responsiveness of the CES model to data changes. As α increases, a higher proportion of data contributes to the predicted value. If a smaller α value is obtained, the historical data has a greater weight value in the predictive model. In this study, we performed experiments with α values of 0.1, 0.5, and 0.9 and found that $\alpha = 0.5$ yielded the best fit to the original data. The prediction effect diagrams are shown in Fig. 2.

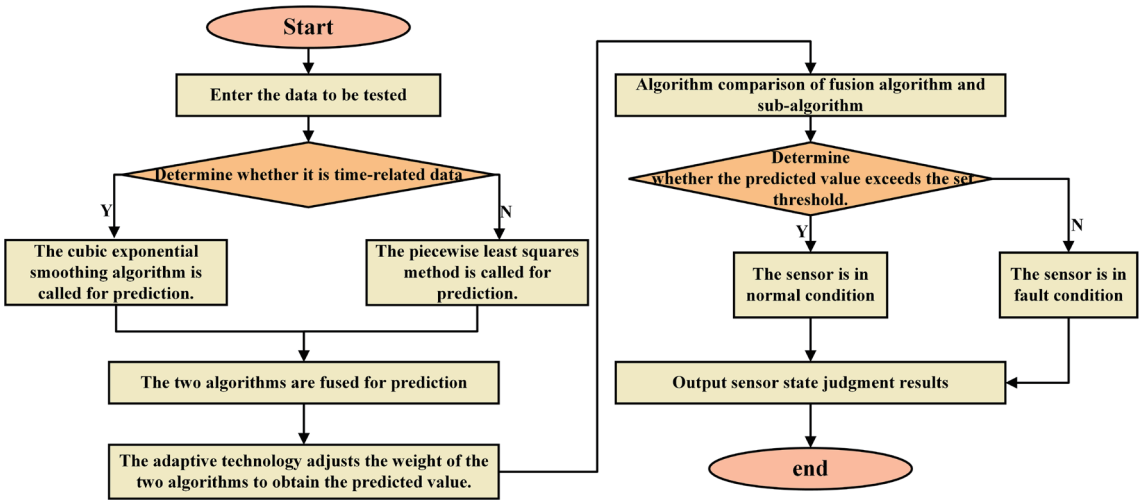

Fig. 1. (Color online) Implementation of spatial-temporal correlation FA.

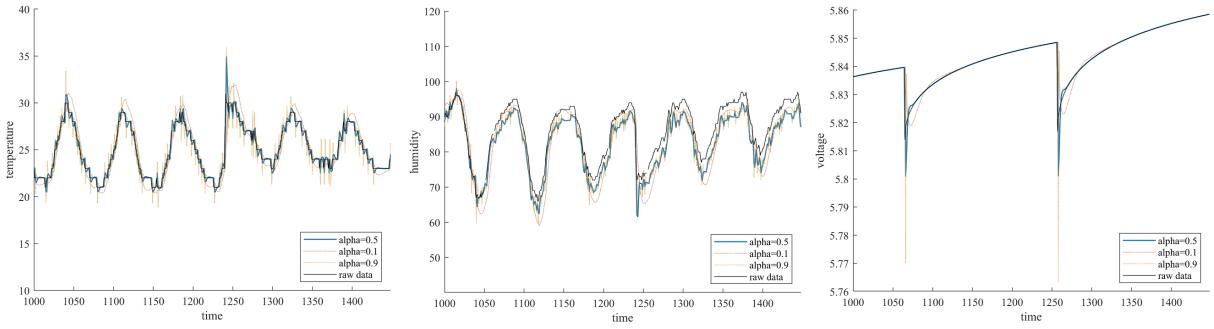

Fig. 2. (Color online) Prediction effects of different smoothing coefficients.

The analysis of the prediction effect of the smoothing coefficient across different values in Fig. 2 reveals that a coefficient of 0.5 yields superior fit results for the entire sensor time series data, effectively capturing data trends. Conversely, a coefficient of 0.9 leads to notable prediction fluctuations around turning points, resulting in significant errors compared with real data. A coefficient of 0.1 exhibits substantial deviations between the fit curve and real data, particularly in predicting mutation points, where the effect is less pronounced.

In summary, selecting 0.5 as the smoothing coefficient by the trial-and-error method can provide a more balanced weight distribution for the data, that is, it provides a balance between the biases of past and latest observations.

3.2 Piecewise points in PLSE method

In time series data, there exists a statistical correlation between consecutive data points, and it changes gradually over time. The direct segmentation of data in chronological order is feasible without the need to identify distinct change points. Given the absence of precise tools or methods to identify points of sharp characteristic changes in statistical data, employing a fixed interval method to track the data's statistical characteristics has proven practical. Hence, in this study, we selected a sliding time window of 100 data points to segment the time series data. Simultaneously, 100 data points serve as segmentation points for the fixed window length, minimizing the overall fit error between predicted and actual data, consistent with the principle of minimum overall fit error. Consequently, the sliding window length of 100 data points can be deemed as the fixed window interval for determining the optimal segmentation point.

3.3 Weight coefficient in FA

In determining the weight coefficient, we employed an adaptive weight adjustment method based on the error between the predicted and original data. This approach dynamically adjusts the weight of each submodel in accordance with recent performance, enhancing the overall prediction accuracy. Adjusting the weights in accordance with the latest performance can assign more appropriate weights to different models at different time points.

The calculation of a single weight is

$$W_1 = \frac{e_1 + e_2}{e_1}, \tag{10}$$

$$W_2 = \frac{e_1 + e_2}{e_2}. \tag{11}$$

With Eqs. (10) and (11), we can calculate the weight values of the CES model and the segmented least squares model in the FA, respectively. e_1 and e_2 are the prediction errors of the CES and PLSE models, respectively, for temperature, humidity, and voltage. The threshold of the prediction error is set in accordance with the performance. If the prediction error of the model for the data is less than the set threshold, then its weight will be larger.

Then, the relative weight is calculated as

$$u = \frac{W_1}{W_1 + W_2}. \tag{12}$$

Equation (12) represents the relative proportion of the two weights, indicating the significance of the CES model compared with the PLSE model. If $W_1 > W_2$, the value of A will approach 1, signifying higher reliability in the prediction results of the CES model. Here, W_1 and W_2 represent the weights calculated using the model based on prediction errors.

The actual weighting coefficient is

$$u^* = u_{t-1} \cdot \mu + u_t(1-\mu), \tag{13}$$

where u_{t-1} is the weighted average of the past, u_t is the current weighted average, and μ is the forgetting factor. By dynamically adjusting the weight and calculating the weighted average, the reasonable consideration of past and new information in the data fusion process can be achieved.

4. Simulation Results and Analysis

4.1 Simulation settings

The simulation hardware environment is 11th Gen Intel® CPU, the operating system is Microsoft® Windows 11 64-bit, and the software environment is Matlab2022b.

For this study, open-source data from agrometeorological station sensors available on the GitHub platform were selected. Although the dataset originates from meteorological monitoring, it fundamentally represents time-series data captured by sensors, which exhibit characteristics that align with the requirements of the spatial-temporal correlation FA employed in this research. The spatial-temporal correlation present in the temperature, humidity, and voltage data supports

the validation of the algorithm's accuracy and robustness. Furthermore, the dataset is open, transparent, and reliable, ensuring high-quality data and the reproducibility of the experimental results. Therefore, it is highly suitable for the simulation and algorithm testing conducted in this study. Table 1 shows a subset of the real-time response data from this dataset, recorded on 22 June 2022.

In the simulation, the order of CES prediction is selected as $N = 3$, the prediction step size of the prediction time point is selected as $p = 1$, and the fixed window length in the PLSE method is 100 data points. The simulation results showed the data from the 1000th time point to the last time point. Because the data fluctuation of the sensor nodes monitored in front of the data set is unclear, the simulation experiment is carried out directly from the data of the 472th time point. The missing values in the collected data set are few and negligible. The simulation results showed the data from the 1000th time point to the last time point.

4.2 Display of results

In the simulation, the temperature, humidity, and voltage monitoring data of the collected sensors are fitted by the CES algorithm, least squares method, and PLSE method, respectively. The fit results are shown in Fig. 3.

Figure 3 shows that the trend of actual sensor data correlates with cyclical and seasonal environmental activities. The CES algorithm adeptly adjusts to data changes by applying unequal weight processing to data at different time nodes, automatically identifying pattern changes and adjusting the prediction model. In the left column of Fig. 3, it is evident that the CES algorithm struggles to track data trend changes at mutation points. Conversely, in the middle and right columns, it is observed that the single least squares method fails to handle numerous nonlinearly changing data points effectively. The PLSE method yields superior fit effects compared with the single least squares method, thereby enhancing the agreement between the model and the data.

Adjacent sensors are typically deployed under comparable environmental conditions. Hence, when employing the PLSE method, environmental data from one sensor can predict that of another sensor. Data distribution indicates a robust spatial correlation between temperature and humidity data among different sensors, whereas the correlation between voltage and temperature/humidity data is weaker.

Table 1
Some data enumeration of the dataset.

Time	Temperature (℃)	Humidity (%)	Voltage (V)
7:07:10	28	85	5.790837
7:07:20	28	85	5.791682
7:07:30	29	84	5.792004
7:07:40	29	83	5.792239
7:07:50	29	82	5.792425
7:08:00	29	82	5.79259
7:08:10	29	81	5.792736

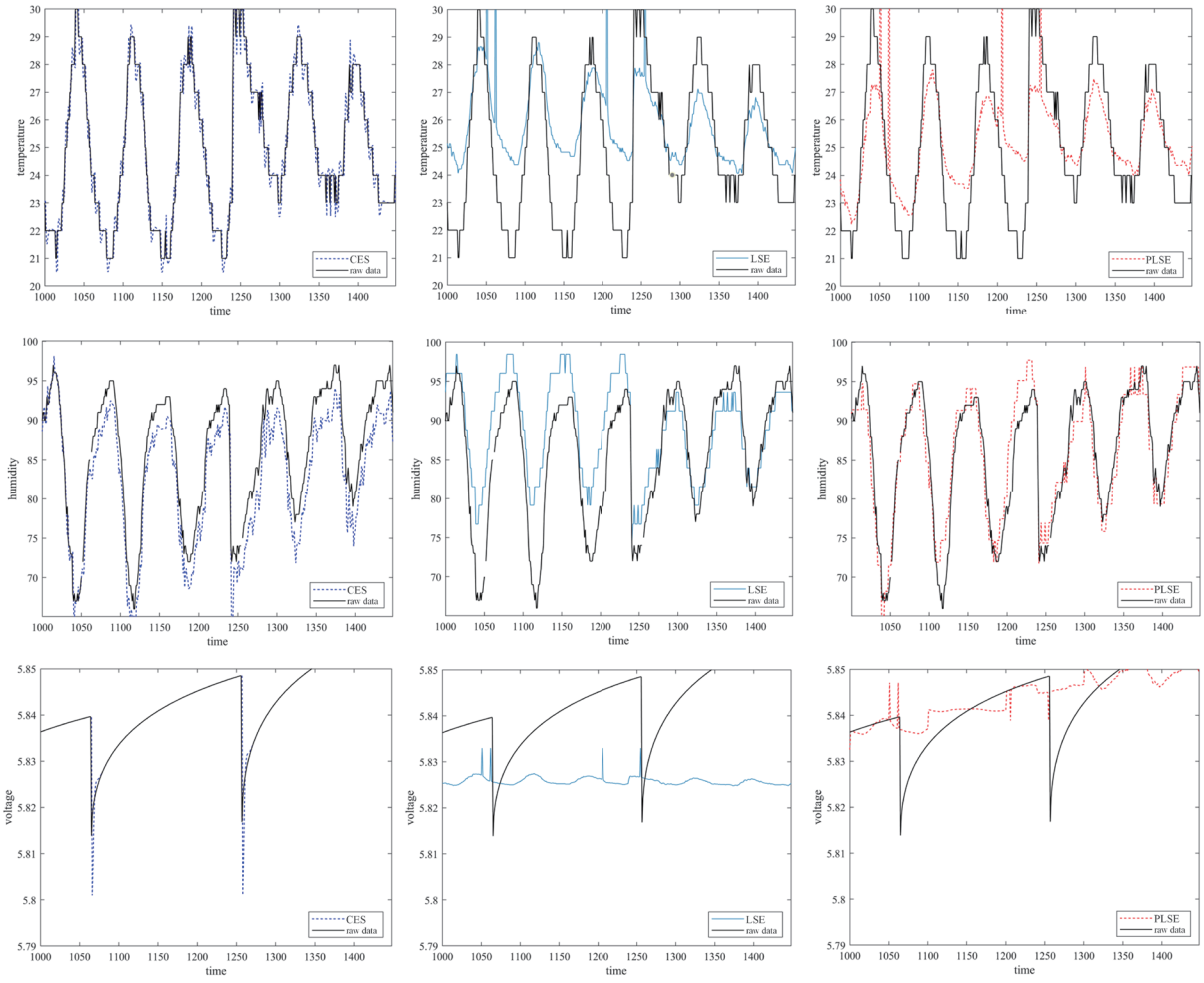

Fig. 3. (Color online) Fitting of different algorithms on sensor data.

4.3 Comparison of FA and subalgorithm

In this study, the CES algorithm, which captures time correlation, and the enhanced PLSE method, representing spatial correlation, are integrated to complement each other's deficiencies. By leveraging their respective strengths, this combined approach aims to achieve superior model performance and enhance the credibility of prediction results.

The exponential smoothing algorithm struggles with nonlinear trends, whereas the PLSE PLSE algorithm excels in capturing them through segmentation. Combining the instantaneous responsiveness of the CES algorithm with the flexible adaptability of the PLSE algorithm maintains sensitivity to recent data while accommodating diverse trends across different time periods, enhancing the adaptability to complex data changes. The comparative diagrams are shown in Fig. 4.

Figure 4 reveals the enhanced FA's clear superiority in predicting actual data, showcasing a high degree of agreement between the model and data points. Nearly all observations closely align with the prediction curve, accurately reflecting the genuine trend and pattern of the data.

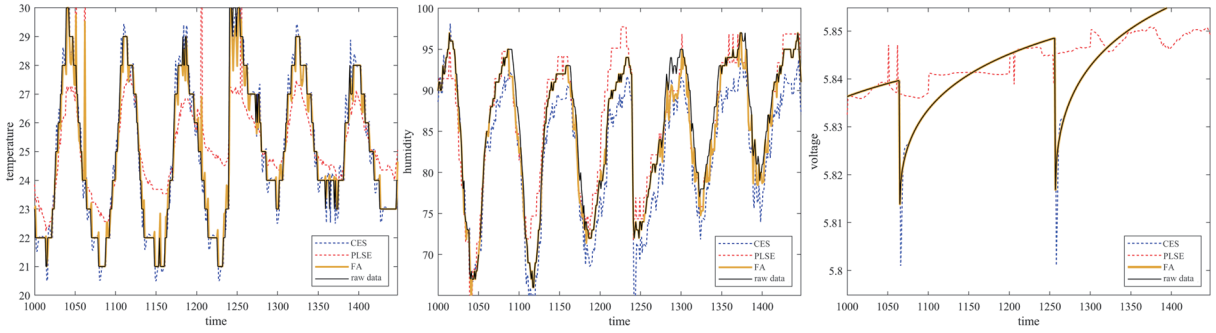

Fig. 4. (Color online) Fittings of FA and subalgorithm.

Table 2
MMSE evaluation of each algorithm.

	Temperature	Humidity	Voltage
CES algorithm	0.4660	1.0116	0.0025
Least squares method	1.2997	4.1554	0.1186
Sub-least squares method	1.1312	2.7798	0.0281
FA	0.2556	0.9366	0.0020
LSTM	1.4986	2.1037	4.0218

Finally, in this study, we use the minimum mean square error (MMSE) algorithm to evaluate the superiority of each algorithm. The specific indicators are shown in Table 2.

The results in Table 1 show that the prediction accuracy of the PLSE estimation algorithm for the actual data is improved compared with that of the single LSE algorithm. From the MMSE value, it can be seen that the PLSE algorithm increases the values of temperature, humidity, and voltage by 13.0, 33.1, and 8.9%, respectively. Then, the MMSE value of the FA is lower than those of the single CES algorithm and PLSE method. For the prediction of temperature data, by calculating the obtained MMSE values, it is known that the FA predictions are 45.1 and 77.4% more accurate than those of the CES and segmented least squares algorithms, respectively.

At the end, the LSTM algorithm is introduced for the prediction of sensor data. By comparing the MMSE values of the FA model with those of the LSTM prediction model, the MMSE value of the FA is found to be 82.9% lower than that of the LSTM for the fit of temperature data. This shows that the FA model has high accuracy and robustness for the prediction of abnormal sensor data.

4.4 Sensor fault detection

The mean absolute error (MMSE value) is used as the threshold, and then the value predicted using the FA is added and subtracted from the MMSE value to obtain the confidence interval, as shown in Fig. 5.

Figure 5 shows that because the fit of the FA is good, the confidence interval based on the results of the FA model and the obtained error value has a certain degree of credibility. When the original data exceeds the set confidence interval, it can be judged that the data is abnormal, that

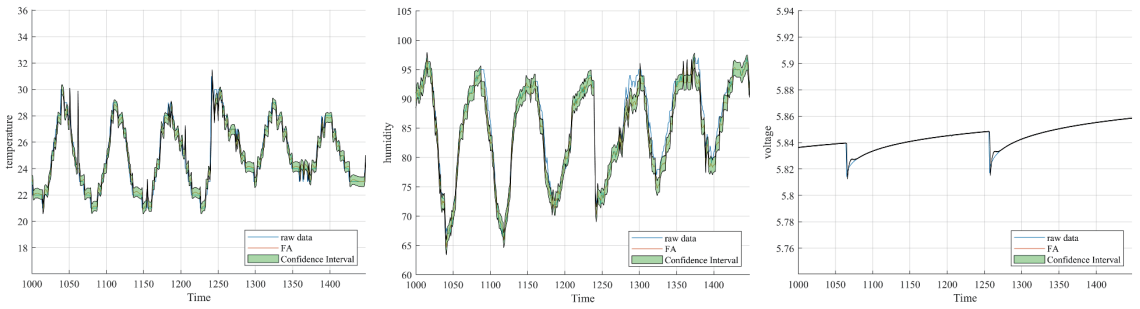

Fig. 5. (Color online) Predicted value and confidence interval.

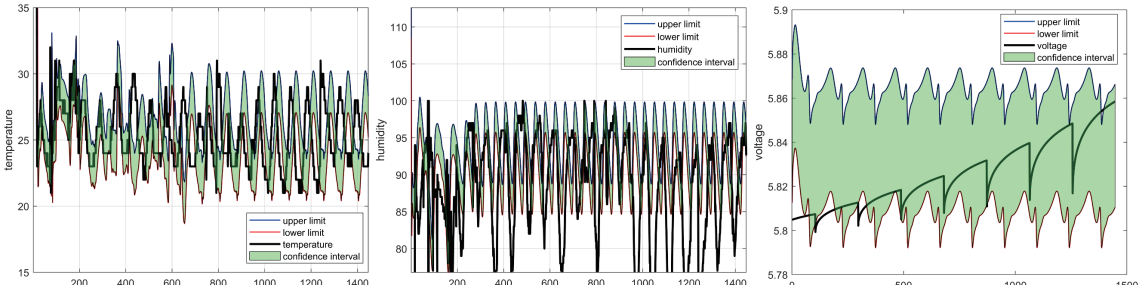

Fig. 6. (Color online) Predictions and confidence intervals for LSTM.

is, the current wireless sensor node is in a fault state. Because the error of the voltage data is small, the confidence interval in the figure is unclear, but the fault node of the wireless sensor can be judged by observing the temperature and humidity data.

First, 80% of the data in the dataset is used as the training data. The feature vector of the data is set to 300, the number of LSTM units is 200, and the learning rate is set to 0.001. The time series model is established by LSTM to predict the temperature, humidity, and voltage in real time. Then, the upper limit is set for each predicted value, that is, 0.5 times the standard deviation of all data before the predicted value is added or subtracted, and the confidence interval is obtained. Figure 6 shows that owing to the low degree of fit of LSTM predictions to the actual data, there is a certain gap between the obtained confidence interval range and the original data, which is inconvenient for detecting the fault sensor.

5. Conclusions

In this study, we addressed the challenge of detecting abnormal data in wireless sensor networks by proposing a novel prediction method based on a spatial-temporal FA. Simulation results demonstrated that the enhanced FA yields superior prediction performance. Specifically, for temperature data, the FA achieved real data fit accuracies that are 45.1 and 77.4% higher than those of the CES and PLSE algorithms, respectively. At the same time, the prediction accuracy of the FA is 82.9% higher than that of the LSTM model, which proves that the FA has higher accuracy for detecting fault sensors in sensor networks.

In terms of sensor fault data detection, although the improved segmented least squares fit improves the overall fault detection capability, there exists a large amount of nonlinear data in the actual monitoring environment, which may cause sufficient accuracy for the prediction of fault data. The focus of subsequent research will be to further improve the fit accuracy of the FA in terms of spatial correlation, so as to achieve more accurate sensor node fault detection and support the effective deployment and application of wireless sensor networks in different application scenarios.

Acknowledgments

This work was supported by the Science and Technology Project of China Southern Power Grid Co., Ltd., under Grant no. YNKJXM20230458.

References

1 F. Z. Wu, J. Yang, H. Jaing, X. P. Zhan, S. Y. Liao, J. Xu, H. Fan, and J. F. Liang: Int. J. Electr. Power Energy Syst. **140** (2022) 108058. https://doi.org/10.1016/j.ijepes.2022.108058
2 L. Ye, Y. Yang, W. Meng, X. Wu, X. Li, and R. Zhu: EURASIP J. Adv. Signal Process. **2024** (2024) 21. https://doi.org/10.1186/s13634-024-01116-4
3 Y. Tsyban, E. Le Roux, A. Fakieh, I. Hoteit, and K. N. Salama: IEEE Sens. J. (2023) 1 https://doi.org/10.1109/SENSORS56945.2023.10325085
4 M. Nazeer, S. Salagrama, and P. Kumar: MethodsX **12** (2024) 102581. https://doi.org/10.1016/j.mex.2024.102581
5 D. Jiang, Y. Ba, and W. Li: J. Beijing Univ. Aeronaut. Astronaut. **49** (2023) 1583. https://doi.org/10.13700/j.bh.1001-5965.2021.0501
6 E. Canzini, M. Auledas, D. Chasteau, and A. Tiwari: IFAC Papersonline **55** (2022) 283. https://doi.org/10.1016/j.ifacol.2022.04.207
7 J. Yang, T. Gao, H. Zhang, and Y. Li: Meas. Sci. Technol. **34** (2023) 125112. https://doi.org/10.1088/1361-6501/acef4a
8 R. Feng and M. Chen: Lect. Notes Artif. Intell. **13532** (2022) 731. https://doi.org/10.1007/978-3-031-15937-4_61
9 C. Zhu, Y. Huang, Q. Liu, L. Zhang, G. C. Liu, and Z. F. Zhou: Power Syst. Big Data **23** (2020) 10. https://doi.org/10.19317/j.cnki.1008-083x.2020.09.002
10 P. Li, Y. Wei, N. Li, T. Huang, and N. Jin: IEEE Sens. J. (2022) 1070. https://doi.org/10.1109/WCSP55476.2022.10039312
11 Y. Seyedi, H. Karimi, S. Grijalva, J. Mahseredjian, and B. Sanso: IEEE Syst. J. **16** (2022) 4060. https://doi.org/10.1109/JSYST.2021.3112710
12 Y. H. Han, Q. Y. Chen, N. Pan, X. J. Guo, and Y. Q. An: Sens. Mater. **34** (2022) 3255. https://doi.org/10.18494/SAM3877
13 Y. Bie, Z. Li, Z. Hu, and J. Chen: IEEE Access **10** (2022) 54313. https://doi.org/10.1109/ACCESS.2022.3163519
14 B. Yang, L. Zhang, B. Zhang, Y. Song, and E. Ding: J. Syst. Eng. Electron. **42** (2020) 2013. https://doi.org/10.3969/j.issn.1001-506X.2020.09.17
15 X. Allamigeon, D. Dadush, G. Loho, B. Natura, L. A. Vegh, and I. C. Soc: Int. J. Found. Comput. Sci. (2022) 267. https://doi.org/10.1109/FOCS54457.2022.00032
16 P. M. R. dos Santos and M. I. R. dos Santos: Simulation **97** (2021) 761. https://doi.org/10.1177/00375497211018734

About the Authors

Yuan Wang graduated from Kunming University of Science and Technology in 2012 with a bachelor's degree in electrical engineering and automation. She is now an engineer and technician in charge of emerging business management at the Chuxiong Power Supply Bureau of Yunnan Power Grid Co., Ltd. Her research interests include key technologies of intelligent logistics and digital management of charging infrastructure. (wangyuan@cx.yn.csg.cn)

Nuobin Zhang is a student in the School of Faculty of Civil Aviation and Aeronautical of Kunming University of Science and Technology and is working toward a bachelor's degree in transportation. At the same time, she is also working as an intern at Yunnan Power Grid Energy Investment Co., Ltd. Her main interests lie in operations research, traffic management, and machine learning. (2972322553@qq.com)

Huijie Wang graduated from Kunming University of Science and Technology in 2009 with a bachelor's degree in electrical engineering and automation. She works in Chuxiong Power Supply Bureau of Yunnan Power Grid Co., Ltd. and is currently an engineer in charge of power saving management. (wanghuijie@cx.yn.csg.cn)

Chunfang Pan graduated from Chuxiong Normal University in 2021 with a bachelor's degree in electrical engineering and automation. She is currently an assistant engineer at the Chuxiong Lucheng Power Supply Bureau of Yunnan Power Grid Co., Ltd. Her main research interests are in the key technologies of intelligent logistics and the digital management of charging infrastructure. (panchunfang@yn.csg.cn)

Jiarui Li is a student in the School of Faculty of Civil Aviation and Aeronautical of Kunming University of Science and Technology and is working toward a bachelor's degree in transportation. At the same time, she is also working as an intern at Yunnan Power Grid Energy Investment Co., Ltd. Her main interests lie in operations research and multi-objective programming. (2602535408@qq.com)